JOURNAL OF Materials CHEMISTRY

# Synthesis and characterisation of dual-phase Y-TZP and $RuO_2$ nanopowders: dense electrode precursors

**Werner E. van Zyl,*[a] Louis Winnubst,[a] Tomas P. Raming,[a] Riaan Schmuhl[a] and Henk Verweij[b]**

[a]*Laboratory for Inorganic Materials Science, Faculty of Chemical Technology and MESA+ Research Institute, University of Twente, P.O. Box 217, 7500 AE Enschede, The Netherlands. E-mail: w.e.vanzyl@ct.utwente.nl*

[b]*Department of Materials Science and Engineering, The Ohio State University, Columbus, OH 43210-1178, USA*

***Received 6th November 2001, Accepted 3rd December 2001***
***First published as an Advance Article on the web 28th January 2002***

The synthesis and characterisation of nanopowders in the dual-phase system tetragonal-$Y_2O_3$-doped $ZrO_2$ (Y-TZP) and $RuO_2$ are described. Five powders were prepared from a co-precipitation (CP) method with stoichiometric variation in the $RuO_2$ content (5–46 mol%) and two powders were prepared from solid-phase mechanical mixing of the above oxides prepared separately. In the CP method, an aqueous chlorometal solution containing appropriate precursor ions was co-precipitated in a concentrated aqueous ammonia (pH $\sim$14) solution. Following filtration, washing and drying (100 °C), the CP synthesis route yielded black coloured amorphous powders. Crystalline dual-phase powders were obtained after calcination in stagnant air at 600 °C for 2 h. The average Y-TZP and $RuO_2$ crystallite sizes were, respectively, 10 and 20 nm, *i.e.* a nano/nano powder. The powders were characterised by X-ray diffraction (XRD), transmission electron microscopy (TEM), backscatter Raman spectroscopy ($ZrO_2$ phase determination) and quantitative X-ray fluorescence (XRF). Time-dependent calcination experiments for samples of similar composition revealed that under the synthesis conditions employed, a composite was formed where a fraction of the crystalline $RuO_2$ phase was initially dissolved in the $ZrO_2$ phase and which gradually transforms to a more stable, distinctly dual-phase system upon prolonged ($\geqslant$20 h) calcination at 600 °C.

## 1. Introduction

Oxide-based nanocrystalline ceramics have found applications in several technological areas such as high-density coatings, catalysis, thin films and electrode devices.[1–4] The high thermal stability (>500 °C), chemical inertness against corrosives and low thermal expansion coefficients make this class of ceramics particularly useful. Advanced single-phase ceramics such as $RuO_2$, $Al_2O_3$ and $BaTiO_3$ are used as conductors, abrasives/insulators and capacitors, respectively. When two or more phases are considered, information on the mutual solubilities of the respective phases is valuable but, together with factors that influence the solubility, not known for most composites. The solubility limit of a dual-phase composite has serious implications in both the physical and chemical properties (and thus perceived applications) that can be expected for the composite. Pure zirconia, for instance, exists in the monoclinic phase at room temperature which then transforms to the tetragonal phase at 1170 °C, and to the cubic phase at 2370 °C. Through addition of appropriate amounts of stabilising oxides such as $Y_2O_3$ or CaO, zirconia can be stabilised in all phases to room temperature. In the case of the tetragonal phase, however, additional microstructural conditions must be met.[5] In the dual-phase system described here, an attempt to quantify the solubility limit is of importance since $RuO_2$ is an electronic conductor while $ZrO_2$ is an electronic insulator. In the event that the former completely dissolves in the latter, forming one phase, all electron conducting properties can be quenched. The metal oxides chosen for the present study comprise $Y_2O_3$-doped $ZrO_2$ (Y-TZP) and $RuO_2$. Ruthenia crystallises in the rutile structure and is one of few oxides that exhibits metallic conductivity on the order of $2 \times 10^4$ S cm$^{-1}$ for anhydrous, single crystals which, along with its thermal and chemical stability, makes the material feasible for nanowire[4] applications in the presence of water and oxygen.[6,7] In addition, $RuO_2$ is a very active electro-catalyst used in the anodic oxidation of chlorine and cathodic reduction of oxygen[8–10] and shows high catalytic activity in the Fischer–Tropsch process.[11] Zirconia is an inert, low-cost, oxygen-ion conducting material[12] that has previously been used as a stabiliser for $RuO_2$ electrode materials[13] and has also been evaluated as a component in a solid oxide fuel cell (SOFC).[14] The powders reported in this study can be compacted to form dense electrodes[15] where the electron conduction not only requires two distinct and separate phases, but also that the mol% $RuO_2$ is equal to or exceeds the percolation limit. Since $RuO_2$ is relatively expensive, it becomes more economically viable the less $RuO_2$ dissolves in the $ZrO_2$ phase.

We have previously reported on the temperature/pressure compaction characteristics for some of the powders reported herein leading to dense electrode devices.[16] Others have reported on the formation of $ZrO_2$–$RuO_2$ powders using different synthesis methods and reporting a variety of solubility limits.[17–21] In this study we report on *i*, the synthesis of Y-TZP/$RuO_2$ powders and describe essential synthesis conditions/parameters to achieve nano-sized grains, *ii*, a composite system whereby the extent of solubility of the $RuO_2$ phase into the $ZrO_2$ phase is a time-dependent phenomenon, as demonstrated by calcination experiments conducted at 600 °C. Since this system has already shown potential and demonstrated technological applications, it is important to know the optimum synthesis conditions for obtaining nano-size particles and to recognise what range of solubility limits can be expected under different experimental conditions.

 DOI: 10.1039/b110107m

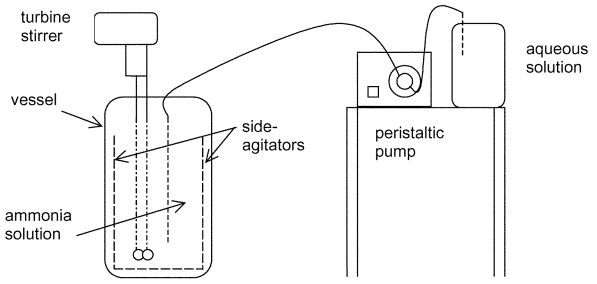


**Fig. 1** Schematic illustration of the reaction apparatus and synthesis set-up for the co-precipitation (CP) method.

## 2. Experimental

### Synthesis

Five powders were prepared from a co-precipitation (CP) method. The synthesis set-up described below can be visualised in Fig. 1. An aqueous solution (1.2 $dm^3$) was prepared from the following chlorometal precursor materials: $ZrOCl_2 \cdot 8H_2O$ (Merck, Germany), $YCl_3$ (Cerac, USA) and $RuCl_3 \cdot xH_2O$ (Acros, Belgium), where $x = 3.4$ as determined by thermogravimetric analysis. The molar percentages of metal ions were varied for each synthesis with a total metal ion concentration in the range 1.7–2.5 M. The CP method described here is suitable for reaction scale-up to yield from 10 g to at least 250 g of dry powder. The dark coloured metal-containing solution (pH $\sim$ 3) was filtered through a 0.025 μm membrane to remove any traces of insoluble species. The solution was then added to 8–9 $dm^3$ of a concentrated aqueous ammonia (pH $\sim$ 14) solution contained in a PTFE-coated stainless-steel vessel ($\phi$ = 25 cm) over a 6 h period. The ammonia solution was stirred vigorously and continuously with a top-mounted turbine stirrer ($\phi$ = 12 cm). Agitation was further enhanced by the placement of PTFE coated metal fins along the inside walls of the vessel. The metal-containing solution was added with the aid of a peristaltic pump through a narrow tube of 1.5 mm diameter. The end of the tube was placed directly above the tip of the stirrer to maximise nucleation sites and minimise nucleus growth. During the addition process, the gradual decrease in basicity was ceased at a minimum pH = 12 through subsequent additions of ammonia. Once all solution had been added, a dispersion-stirrer replaced the turbine-stirrer and the suspension was stirred for an additional 1 h. The resulting mixture was then poured into a glass vessel. Subsequent XRF data showed no traces of silicon species that leached into the solution. The mixture was sealed and left to sedimentate overnight. The settling of fine particles should become apparent within hours, leaving a colourless solution above the settled gel. If a dark solution remains with only small amounts of precipitated material, it implies that the pH was not maintained at a high enough value and results not only in yield losses but alters the composition of the composite. This situation cannot be remedied by post-addition of large volumes of ammonia. The clear and colourless strongly basic solution was then decanted into a separate flask. The remaining wet black gel was filtered and washed with copious amounts of distilled water to remove most chloride ions. Water washing was continued until the pH had decreased to 9; the pH could not be further decreased without the risk of re-dissolving the precipitated gel. The precipitate was washed with ethanol until the density of the filtrate was below 0.79 g $cm^{-3}$ (*i.e.* water content < 5%). The black coloured gel, suspended in ethanol, was then oven-dried overnight at 100 °C. The resulting amorphous powder was ground in a mortar and then calcined at 600 °C in stagnant air for 2 h at a heating rate of 2 °C $min^{-1}$. Calcining for $\geqslant$ 20 h leads to different compositions (see dicussion).

Apart from the CP method described, two composite powders were also prepared from mixing of separately prepared Y-TZP and $RuO_2$ powders using pre-determined stoichiometries for each phase. These composites are designated MX-powders and they provided useful XRD data for solubility limit comparisons with CP powders since no dissolution can occur from this room temperature dry-mixing process.

### Powder characterisation

The bulk chemical compositions of the composites were determined by quantitative X-ray fluorescence (XRF). XRF analyses were performed on a Philips PW 1480/10-fluorometer (Eindhoven, The Netherlands). Samples were prepared for measurement by pressing the powders with the use of a binder into a tablet. The measurement method has been described previously.[22]

Powder X-ray diffraction (XRD) and X-ray line broadening (XRLB) measurements characterised the $ZrO_2$ and $RuO_2$ components. Two types of diffractometers were utilised. The amorphous-to-crystalline transitions were monitored from variable temperature XRD data obtained on a Philips X'Pert MPD HTK-16 (Anton Paar) diffractometer (Eindhoven, The Netherlands), fitted with a Cu-tube and a secondary curved graphite monochromator. A few milligrams of each uncalcined powder were dispersed on a Pt-foil. The foil was heated in a high temperature XRD (HT-XRD) chamber at a rate of 2 °C $min^{-1}$. The temperature was raised with 100 °C increments and kept constant for 2 h at each interval after which the XRD spectrum of the powder was measured *in situ*. Following the final measurement at 700 °C, the powder was cooled to room temperature where another XRD measurement was performed. Data for the phase composition of the calcined powders were collected at room temperature with a Philips X'Pert-1 PW3710 diffractometer (Eindhoven, The Netherlands), using Cu-K$\alpha$ ($\lambda$ = 1.542 Å) radiation. The same apparatus was used to measure the X-ray line broadening (XRLB) to determine the average crystallite size of the respective phases with the Scherrer formula.[23]

Transmission electron microscopy (TEM) was performed with a Philips EM30 Twin TEM (Eindhoven, The Netherlands) to determine the bulk morphology and crystallite sizes. Characterised samples were prepared in an alcohol suspension and dispersed by ultra-sonification for 10 min. One drop of the suspension was added to a copper grid that was air-dried prior to use.

Backscatter Raman spectra were recorded from an Ar–Kr mixed gas laser operating at 488 nm. The laser was coupled with a Coherent 70 Innova spectrum detector (LN/CCD 1100 PB/VISAR, Princeton Instruments Inc.,Trenton, NJ, USA). A backscatter geometry was used with a pinhole width of 50 μm and a laser intensity of approximately 5 mW. The equipment set-up is described more extensively elsewhere.[24]

The crystallisation behaviour of the amorphous zirconia containing powders was also determined with differential scanning calorimetry (DSC). Approximately 50 mg of each uncalcined powder was heated in air at a rate of 10 °C $min^{-1}$ to 700 °C or 750 °C in an alumina crucible using a Setsys-18 thermal analyser with a DSC-1500 measuring head (Setaram, France). Upon reaching the highest programmed temperature, the powders were cooled immediately. The phase composition of the powders after the DSC measurements was verified with XRD.

## 3. Results and discussion

### Synthesis of nanopowders

The synthesis method and apparatus set-up utilised in this study was aimed at forming homogeneously distributed

nano-size grains. Another aim was to gain an understanding of the solubility limit of the system and the factor(s) that influences that solubility. Chloro-metal salts were used as precursors throughout since they are readily soluble in water, leading to a clean precipitation event, that is, controlled at the molecular level. An all-chloro counter-ion methodology also limits other ions as potential sources for contamination. The use of chloro salts also meant that the whole procedure could be performed at room temperature and no extended reflux periods are necessary, as in the case of $Ru(acac)_3$.[17] Independent studies by us showed that when the prepared solution was added fast and with minimal agitation, then inhomogeneous, large grained precipitated powders resulted. To obtain nano-size primary particles, our set-up ensured maximal nucleation sites (rigorous stirring) and minimal grain growth. To ensure that the precipitated material (mainly the '$Ru(OH)_4$'-based species) did not re-dissolve, it was imperative to retain the reaction mixture at high pH (13–14) for the duration of the synthesis.

In the following section, a brief overview will be given of synthesis methods employed by others as well as the estimated solubility limits obtained. The results we obtained will then be described and compared in subsequent sections. The $ZrO_2$–$RuO_2$ system demonstrates that synthesis and processing conditions (starting materials, acid *vs.* alkaline media, stirring rate and rate of addition, calcination time and temperature, *etc.*) have a large influence on the eventual composition and morphology of the powders obtained. Colomer and Jurado reported the solid-state solution $[(ZrO_2)_{0.92}(Y_2O_3)_{0.08}]_{1-x}$-$(RuO_2)_x$ ($0 \leqslant x \leqslant 0.3$ mol) obtained by a polymeric sol–gel process from non-halogenated precursor metal salts.[17] Using powder XRD as a characterisation tool, it was claimed that the solubility of $RuO_2$ in $ZrO_2$ for this system was 8–10 mol% after 2 h calcination at temperatures up to 500 °C. We obtained a similar result for high loadings of $RuO_2$. Their synthesis method has inherent disadvantages, however, such as requiring 10 d of constant refluxing at elevated temperatures, which inevitably leads to very large grains (>500 μm) and inhomogeneously distributed agglomerates. A major difference in that system[17] too is the use of an acidic medium with $HNO_3$ as hydrolysing agent, whereas our system was prepared in a highly basic medium. This difference may play an important role in the final composition of the system. In addition, a cubic $ZrO_2$ phase was obtained while our method exclusively led to a tetragonal $ZrO_2$ phase.

Djurado *et al.* investigated the related system $[(ZrO_2)_{0.91}$-$(Y_2O_3)_{0.09}]_{1-x}(RuO_2)_x$ ($0 \leqslant x \leqslant 0.2$ mol).[19] An aqueous solution that contained nitrate-based salts of Ru, Zr, and Y was dried and subsequently calcined at 900 °C for 12 h to decompose all $NO_x$ gases. The solubility of $RuO_2$ in $ZrO_2$ was subsequently found (by XRD) to be 10–12.5 mol%. The authors concluded that "the best compromise between thermal stability and crystallinity appears to be achieved with calcination at 900 °C'. Our studies revealed that under those calcination conditions for a nanostructured powder, a portion of the $RuO_2$ would irreversibly sublime as $RuO_4$ gas out of the composite, changing the composition dramatically.[16] Other worrisome indicators in that study were the unfortunate choice of internal reference material, namely Si, which has a (111) peak at $2\theta = 28.44°$ while that for $RuO_2$ (110) lies at $2\theta = 28.02°$ (both $I = 100\%$), leaving room for overlap and thus unreliable solubility values. Furthermore, in a time-dependent study at 1100 °C, they assigned the $RuO_2$ (111) 'right shoulder' at $2\theta = 35.20°$, while (111) lies at $2\theta = 40.55°$.[26] If $RuO_2$ (101) is meant at $2\theta = 35.065°$ ($I = 77\%$) then it should be a 'left-shoulder' due to overlap with the c-$ZrO_2$ (200) peak at $2\theta = 35.20°$ ($I = 25\%$).[26] Wold and co-workers[20] used the same synthesis route as Djurado[19] but found a solubility limit of 10–15 mol % (850 °C after 12 h calcination) for the pseudo-ternary system $ZrO_2$–$La_2O_3$–$RuO_2$. They dissolved the nitrates in water and obtained evaporation with stirring at 100 °C. Unfortunately, in both cases, no post-calcination bulk analyses of the material have been provided to compare initial with final compositions. Nevertheless, despite different preparation and processing parameters, the results of Colomer,[17,18] Djurado[19] and Wold[20] are in agreement and indicate a solubility limit of *ca.* 10 mol% $RuO_2$ in both undoped $ZrO_2$ and $Y_2O_3$-doped $ZrO_2$ when using a bulk precipitation method with non-halogenated starting materials.

Comninellis, however, reported that no mixed-phase exists in the system undoped $ZrO_2/RuO_2$.[21] The conclusion was based on XRD data obtained from the precipitation of mixed solutions of aqueous $RuCl_3$ and $ZrOCl_2$ that were calcined at 460 °C. Other reports are in agreement with the latter results and stated that heating a composite obtained from dry powder mixing of $RuO_2$ and $ZrO_2$ powders does not lead to dissolution of one oxidic phase into the other.[15,25] The above arguments show that different synthesis strategies have a large influence on the solubility limits in the $ZrO_2$–$RuO_2$ system and hence the phase composition of the final composite.

## Quantitative XRF, XRD and DSC measurements

The molar compositions of the seven powders prepared in this study were determined by quantitative XRF. The results are shown in Table 1.

The amorphous-to-crystalline transition was investigated with high temperature XRD (HT-XRD). The CP46 powder was chosen for this purpose since the two phases co-exist in approximately equal ratios. The obtained spectra are shown in Fig. 2; the Pt peak refers to Pt-foil[26] which also caused diffraction during data collection. The crystallisation temperature of the $ZrO_2$ phase increased from 400 °C for single phase Y-TZP powder to between 500–600 °C for this dual-phase powder, while $RuO_2$ was semi-crystalline already at 300 °C. A major crystalline $ZrO_2$ phase can be observed at 600 °C as well as some amorphous phase. At room temperature this powder (Fig. 2) only shows a Pt-metal peak and a pattern which is

**Table 1** Quantitative XRF data showing the molar percentage composition of Y-TZP and $RuO_2$ nanocomposite powders from CP and MX synthesis methods after calcination at 600 °C for 2 h

| Powder | $RuO_2$ | $ZrO_2$ | $Y_2O_3$ | $HfO_2$ | Cl |
|---|---|---|---|---|---|
| CP46 | 46.6 | 49.7 | 3.1 | 0.5 | 0.1 |
| CP33 | 33.0 | 63.0 | 3.2 | 0.6 | 0.2 |
| CP15 | 15.1 | 79.4 | 4.1 | 1.0 | 0.4 |
| CP9 | 9.3 | 85.0 | 4.7 | 1.1 | 0.0 |
| CP5 | 4.7 | 89.5 | 4.6 | 1.2 | 0.0 |
| MX11 | 11.0 | 83.8 | 4.1 | 1.1 | 0.0 |
| MX5 | 5.1 | 89.6 | 4.2 | 1.2 | 0.0 |

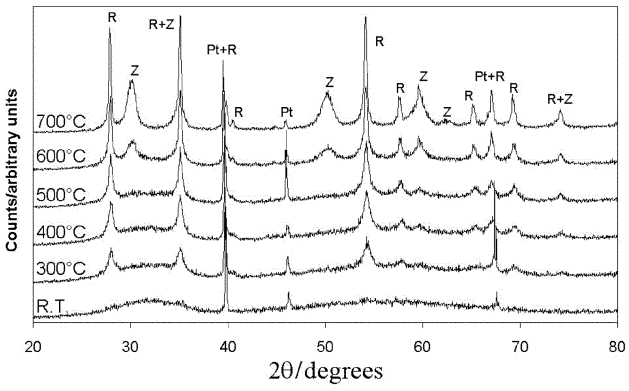


**Fig. 2** High temperature XRD spectra of CP46 composite after initial drying at 100 °C showing the temperature(s) of the amorphous-to-crystalline phase transition. Pt = Pt-foil, Z = $ZrO_2$, R = $RuO_2$.

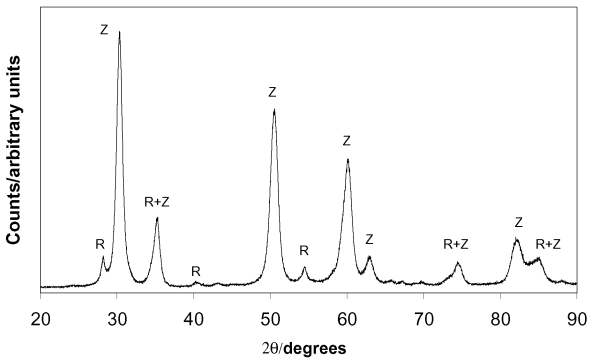


**Fig. 3** XRD spectrum of the CP9 composite after calcination at 600 °C. R = $RuO_2$, Z = $ZrO_2$.

typical for amorphous $Zr(OH)_4$ species.[27] The amorphous phase is characterised by powder XRD through two broad peaks at $2\theta$-values at *ca.* 32° and 55°. Analysis of all XRD spectra, particularly the $ZrO_2$ (111), (222) and (400) reflections, indicated a tetragonal $ZrO_2$ phase.[26] The composite was subsequently investigated with Raman spectroscopy which verified the XRD data. In all cases the crystallisation of $ZrO_2$ occurred at a higher temperature than $RuO_2$. The XRD spectrum of the CP9 powder is shown in Fig. 3 after calcination at 600 °C.

Differential scanning calorimetry (DSC) measurements performed on the CP-powders showed that the crystallisation of $ZrO_2$ was inhibited by the presence of $RuO_2$. The larger the $RuO_2$ content, the higher the crystallisation temperature of $ZrO_2$. DSC showed that the onset-temperature of $ZrO_2$ crystallisation was increased from 426 °C (with a heating rate of 10 °C $min^{-1}$) for the one-phase Y-TZP, to 652 °C for CP46. With HT-XRD the single-phase amorphous Y-TZP powder showed the first crystalline zirconia at 400–450 °C, in accordance with the DSC results.

In the HT-XRD of the dual-phase powders CP33 and CP15, crystallisation of Y-TZP was observed at 500 °C, while for the CP46 powder (see Fig. 2) crystallisation was observed at 600 °C.

### Raman spectroscopy: $ZrO_2$ phase elucidation

Although $RuO_2$ and $ZrO_2$ are both Raman-active oxides, $RuO_2$ is a poor Raman scatterer when combined with other phases, leading to very weak or undetected intensities. We investigated the CP33 powder and present the first Raman spectrum of such composites in Fig. 4. Due to the large 'dilution' effect of the $RuO_2$ phase, we observed an absence of the common symmetry allowed $E_g$, $A_{1g}$ and $B_{2g}$ modes at, respectively, 521, 638 and 705 $cm^{-1}$ found for pure $RuO_2$ phase.[4] The mol% $RuO_2$ present in the bulk composite was already established by other means and so the absence of $RuO_2$ peaks was of secondary importance since the primary aim was to examine which was the major $ZrO_2$ phase. Zirconia occurs in three common phases: monoclinic, tetragonal and cubic. Monoclinic phase can be discarded as neither the $Y_2O_3$ dopant concentration, nor XRD peaks or Raman investigations, are in accord with the monoclinic phase. Prior to Raman studies, the zirconia phase was tentatively assigned as tetragonal based on XRD data. However, since all powder grain sizes were small (<20 nm) on average, the problem of signal broadening in the XRD spectrum was amplified, especially where signal splitting or overlap occurred. In order to obtain supporting evidence for the tetragonal phase observed by XRD, we resorted to Raman spectroscopy.

A sample of pure 3Y-TZP was run and the expected tetragonal phase peaks (all strong intensities) at 642, 463, 314 and 267 $cm^{-1}$ are present.[28] There was a clear resemblance between the pure tetragonal phase and the CP33 composite. The cubic phase[29] has only one (medium) intensity peak at 625 $cm^{-1}$. This peak was somewhat obscured as it resided beneath a portion of a peak assigned to the tetragonal phase; no trace of the cubic peak could be observed. Therefore, since no cubic phase could be detected with XRD also, we concluded that the tetragonal phase was the major phase. Note that the signals for zirconia, which is an efficient Raman scatterer, become broad and appear to shift to slightly lower wavenumbers upon 'dilution' with other oxides.

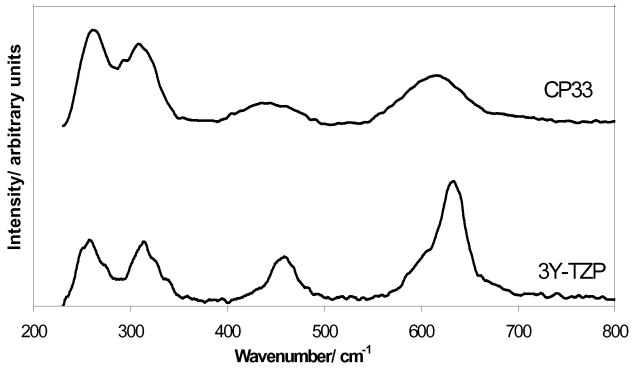


**Fig. 4** Backscatter Raman spectra of pure 3Y-TZP and CP33 powders after calcination at 600 °C.

### TEM characterisation: morphology of the powders

The morphology of the powders was investigated with TEM. A TEM micrograph of CP9 is shown in Fig. 5. Individual crystallites are clearly present. Furthermore, the following conclusions can be extracted from the TEM micrograph: *i*, the particles are mainly spherical in shape and the composite is crystalline as best observed by the multitude of lattice fringes present; *ii*, the particles are on average in the 10–20 nm size regime, which is also verified by XRLB.

### Evidence for time-dependent dual-phase formation

As discussed previously, the solubility limit for the $ZrO_2$–$RuO_2$ system appears to be sensitive to synthesis conditions, which has consequences for eventual application of the material. We endeavoured to at least (semi-)quantify the solubility limit of

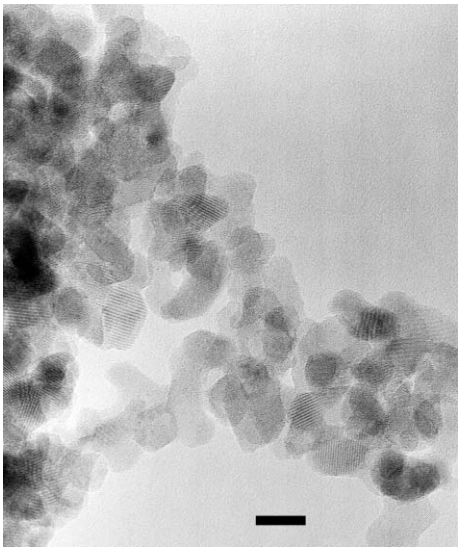

**Fig. 5** TEM micrograph of CP9 composite after calcination at 600 °C. Scale bar = 10 nm.

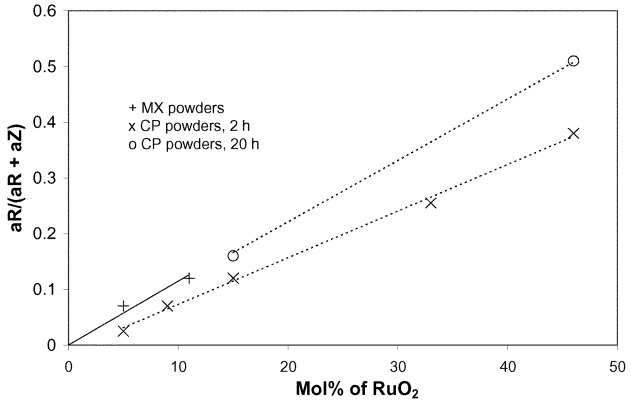


**Fig. 6** The mol% of $RuO_2$ soluble in the $ZrO_2$ phase for different synthesis methods and different calcination (600 °C) times.

this system as follows. Quantitative powder XRD data were analysed by calculating the total area for prominent peaks of post-calcined $RuO_2$ and $ZrO_2$ phases. The peak area of $RuO_2$ (110) [labelled: aR] was divided by the sum of that peak and the $ZrO_2$ (111) peak area [aZ] for both the CP and MX prepared samples. The value obtained from [(aR)/(aR)+(aZ)] was used as a measure to estimate the relative amount of $RuO_2$ phase present, and to compare changes that occur under different experimental conditions. Following this formula we plotted the data points as shown in Fig. 6. No solubility was expected for the MX powders and therefore the MX trendline was extrapolated through the origin. The datapoints ($\times$) originally found on the CP line were compared with the MX line to calculate the amount of $RuO_2$ in Y-TZP as a function of Ru content. One aspect of this line remained puzzling: why was the extended CP trendline not parallel to the MX line where no solid-phase dissolution took place? A related topic questioned why did the DSC results (heating rate: 10 °C $min^{-1}$) show a different amorphous-to-crystalline transition temperature compared to the HT-XRD (2 °C $min^{-1}$) data when the only difference was the amount of time for which the sample was exposed to air at high temperature? These questions encouraged further investigation, which subsequently revealed that both aspects could be explained by a time-dependent phenomenon. The calcination time for powders CP15 and CP46 was increased from 2 to 20 h and the data were analysed in the same manner as discussed. The trendline ($\bigcirc$) that represented 20 hour calcination was almost an extension of the MX-line, implying that upon prolonged calcination almost no $RuO_2$ remained dissolved in the Y-TZP matrix, see Fig. 6. It appeared that a time-dependent demixing of phases was operative. The observation was explained as the formation of an initial solid phase (600 °C, 2 h), where a certain amount of $RuO_2$ was dissolved in the $ZrO_2$ phase, which then transformed to a more stable phase (600 °C, $\geqslant$20 h) upon prolonged calcination time while other experimental conditions remained the same. Particular care was taken to ensure no or minimal monoclinic-$ZrO_2$ phase evolved during the prolonged heating. An assumption was made that the $RuO_2$ phase was crystalline after 2 h calcination at 600 °C which seemed reasonable based on HT-XRD and DSC results. The solubility after 2 h of calcination at 600 °C appeared to be a function of the percentage Ru-species introduced during co-precipitation, but the exact quantity, even though it has to be a fixed (maximum) percentage, is not known.

If, following relatively harsh calcination conditions, the solubility limits of 10 mol% $RuO_2$ claimed by others[17–20] are accurate, we propose, based on the present study, that those systems will also segregate into two distinct phases upon prolonged calcination time.

## 4. Conclusions

Formation of several dual-phase nanopowders consisting of Y-TZP and $RuO_2$ was achieved through a co-precipitation method with large variation in mol% $RuO_2$ added. Following calcination at 600 °C the CP powders were crystalline and consisted of average primary grain sizes of 10 nm for Y-TZP and 20 nm for $RuO_2$, as observed by XRLB and verified with TEM. The crystallisation temperature of the $ZrO_2$ phase increased with the amount of $RuO_2$ present. The $ZrO_2$ phase crystals in all powders are tetragonal as expected by the loading percentage of the dopant, as verified by XRD data and further supported by backscatter Raman spectroscopy. The system described in this study was susceptible to a time-dependent demixing of two phases which initially formed a 'solid solution' with variable amounts of $RuO_2$ dissolved in the $ZrO_2$ lattice, depending on synthesis conditions and initial ruthenia loading percentage. Two well-defined phases appeared after prolonged calcination at 600 °C. Investigations into the explosive ('shock') compaction behaviour of these powders are currently underway in an attempt to obtain dense electrodes, hopefully with retention of the powder characteristics (nano-size, crystallinity, *etc.*) reported herein.

## Acknowledgement

We are indebted to W. Lengton for helpful discussions, Y. Aksenov for performing the Raman measurements and Dr. Stein at the Max-Planck Institute in Düsseldorf for performing the DSC-measurements. We gratefully acknowledge the Netherlands Organisation for Scientific Research (NWO) group of Chemical Sciences (CW) for financial support.

## References

1 F. C. M. Woudenberg, W. F. C. Sager, N. G. M. Sibelt and H. Verweij, *Adv. Mater.*, 2001, **13**, 514.
2 A. J. Zarur and J. Y. Ying, *Nature*, 2000, **404**, 65.
3 J. H. Fendler, in *Nanoparticles and Nanostructured Films*, Wiley-VCH, Weinheim, 1st edn., 1998, p. 429.
4 J. V. Ryan, A. D. Berry, M. L. Anderson, J. W. Long, R. M. Stroud, V. M. Cepak, V. M. Browning, D. R. Rolison and C. I. Merzbacher, *Nature*, 2000, **406**, 169.
5 R. C. Garvie, *J. Phys. Chem.*, 1965, **69**, 1238.
6 S. Ardizzone and S. Trasatti, *Adv. Colloid Interf. Sci.*, 1996, **38**, 173.
7 S. Trasatti and G. Lodi in *Electrodes of Conductive Metallic Oxides, Part B*, Elsevier, Amsterdam, 1981, ch. 10.
8 A. T. Kuhn and C. S. Mortimer, *J. Electrochem. Soc.*, 1973, **120**, 231.
9 A. Bandi, I. Mihelis, E. Vartires, E. Ciortan and I. Rosu, *J. Electrochem. Soc.*, 1987, **134**, 1982.
10 K. Ogura and M. Takagi, *Solar Energy*, 1986, **37**, 41.
11 S. R. Morris, R. B. Moyes and P. B. Wells in *Metal Support and Metal Additive Effects in Catalysis*, ed. B. Imelik, Elsevier, Amsterdam, 1982, p. 247.
12 S. Jiang, W. A. Schulze, V. R. W. Amarakoon and G. C. Stangle, *J. Mater. Res.*, 1997, **12**, 2374.
13 L. D. Burke and M. McCarthy, *Electrochim. Acta.*, 1984, **29**, 211.
14 M. Hrovat, J. Holc and D. Kolar, *Solid State Ionics*, 1994, **68**, 99.
15 T. P. Raming, PhD Thesis University of Twente, Enschede, The Netherlands, 2000.
16 T. P. Raming, W. E. van Zyl and H. Verweij, *Chem. Mater.*, 2001, **13**, 284.
17 M. T. Colomer and J. R. Jurado, *J. Non-Cryst. Solids*, 1997, **217**, 48.
18 M. T. Colomer and J. R. Jurado, *J. Solid State Chem.*, 1998, **141**, 282.
19 E. Djurado, C. Roux and A. Hammou, *J. Eur. Ceram. Soc.*, 1996, **16**, 767.
20 Y. C. Long, Z. D. Zhang, K. Dwight and A. Wold, *Mater. Res. Bull.*, 1988, **23**, 631.
21 Ch. Comninellis and G. P. Vercesi, *J. Appl. Electrochem.*, 1991, **21**, 335.

22 M. Bos, J. A. M. Vrielink and W. E. van der Linden, *Anal. Chim. Acta*, 2000, **412**, 203.
23 P. Scherrer, *Goett. Nachr.*, 1918, **2**, 98.
24 N. M. Sijtsema, Ph. D. Thesis University of Twente, Enschede, The Netherlands, 1997.
25 M. Hrovat, S. Bernik and J. Holc, *J. Mater. Sci. Lett.*, 1999, **18**, 1019.
26 JCPDS-International Centre for Diffraction Data: Pt metal (#04-0802); $RuO_2$ (#43-1027); *t*-$ZrO_2$ (#17-0923); c-$ZrO_2$ (#27-0997); Si (#27-1402).
27 G. T. Mamott, P. Barnes, S. E. Tarling, S. L. Jones and C. J. Norman, *Powder Diffr.*, 1988, **3**, 234.
28 G. Stefanic, S. Music, S. Popovic and A. Sekulic, *J. Mol. Struct.*, 1997, **408/409**, 391.
29 C. M. Phillippi and K. S. Mazdiyasni, *J. Am. Ceram. Soc.*, 1971, **54**, 254.